Spectral analysis based on compressive sensing in nanophotonic structures

Zhu Wang and Zongfu Yu*

Department of Electrical and Computer Engineering, University of Wisconsin, Madison, WI 53705, USA
**zyu54@wisc.edu*

Abstract: A method of spectral sensing based on compressive sensing is shown to have the potential to achieve high resolution in a compact device size. The random bases used in compressive sensing are created by the optical response of a set of different nanophotonic structures, such as photonic crystal slabs. The complex interferences in these nanostructures offer diverse spectral features suitable for compressive sensing.

OCIS codes: (300.6190) Spectrometers; (050.5298) Photonic crystals.

References and links

1. X. Gan, N. Pervez, I. Kymissis, F. Hatami, and D. Englund, "A high-resolution spectrometer based on a compact planar two dimensional photonic crystal cavity array," Appl. Phys. Lett. **100**(23), 231104 (2012).
2. Z. Xia, A. A. Eftekhar, M. Soltani, B. Momeni, Q. Li, M. Chamanzar, S. Yegnanarayanan, and A. Adibi, "High resolution on-chip spectroscopy based on miniaturized microdonut resonators," Opt. Express **19**(13), 12356–12364 (2011).
3. E. J. Candes, J. Romberg, and T. Tao, "Robust uncertainty principles: exact signal reconstruction from highly incomplete frequency information," IEEE Trans. Inf. Theory **52**(2), 489–509 (2006).
4. S. G. Johnson, S. Fan, P. R. Villeneuve, J. D. Joannopoulos, and L. A. Kolodziejski, "Guided modes in photonic crystal slabs," Phys. Rev. B **60**(8), 5751–5758 (1999).
5 P. B. Fellgett, *The Theory of Infrared Sensitivities and Its Application to Investigations of Stellar Radiation in the Near Infra-red*, Thesis (1951).
6. M. F. Duarte, M. A. Davenport, D. Takhar, J. N. Laska, T. Sun, K. F. Kelly, and R. G. Baraniuk, "Single-pixel imaging via compressive sampling," IEEE Signal Process. Mag. **25**(2), 83–91 (2008).
7. L. Zhu, W. Zhang, D. Elnatan, and B. Huang, "Faster STORM using compressed sensing," Nat. Methods **9**(7), 721–723 (2012).
8. C. M. Watts, D. Shrekenhamer, J. Montoya, G. Lipworth, J. Hunt, T. Sleasman, S. Krishna, D. R. Smith, and W. J. Padilla, "Terahertz compressive imaging with metamaterial spatial light modulators," Nat. Photonics **8**(8), 605–609 (2014).
9. O. Katz, Y. Bromberg, and Y. Silberberg, "Compressive ghost imaging," Appl. Phys. Lett. **95**(13), 131110 (2009).
10. W. L. Chan, K. Charan, D. Takhar, K. F. Kelly, R. G. Baraniuk, and D. M. Mittleman, "A single-pixel terahertz imaging system based on compressed sensing," Appl. Phys. Lett. **93**(12), 121105 (2008).
11. A. Shabani, R. L. Kosut, M. Mohseni, H. Rabitz, M. A. Broome, M. P. Almeida, A. Fedrizzi, and A. G. White, "Efficient measurement of quantum dynamics via compressive sensing," Phys. Rev. Lett. **106**(10), 100401 (2011).
12. A. Szameit, Y. Shechtman, E. Osherovich, E. Bullkich, P. Sidorenko, H. Dana, S. Steiner, E. B. Kley, S. Gazit, T. Cohen-Hyams, S. Shoham, M. Zibulevsky, I. Yavneh, Y. C. Eldar, O. Cohen, and M. Segev, "Sparsity-based single-shot subwavelength coherent diffractive imaging," Nat. Mater. **11**(5), 455–459 (2012).
13. "l1_magic". *http://statweb.stanford.edu/~candes/l1magic/*. [Accessed: 10-Jul-2014].
14. E. J. Candes and T. Tao, "Decoding by linear programming," IEEE Trans. Inf. Theory **51**(12), 4203–4215 (2005).
15. S. G. Johnson, S. Fan, P. R. Villeneuve, J. D. Joannopoulos, and L. A. Kolodziejski, "Guided modes in photonic crystal slabs," Phys. Rev. B **60**(8), 5751–5758 (1999).
16. S. Fan, W. Suh, and J. D. Joannopoulos, "Temporal coupled-mode theory for the Fano resonance in optical resonators," J. Opt. Soc. Am. A **20**(3), 569–572 (2003).
17. S. Fan, "Sharp asymmetric line shapes in side-coupled waveguide-cavity systems," Appl. Phys. Lett. **80**(6), 908 (2002).
18. C. Wu, A. B. Khanikaev, R. Adato, N. Arju, A. A. Yanik, H. Altug, and G. Shvets, "Fano-resonant asymmetric metamaterials for ultrasensitive spectroscopy and identification of molecular monolayers," Nat. Mater. **11**(1), 69–75 (2012).
19. V. Liu and S. Fan, "S4 : A free electromagnetic solver for layered periodic structures," Comput. Phys. Commun. **183**(10), 2233–2244 (2012).

#219981 - $15.00 USD Received 29 Jul 2014; revised 12 Sep 2014; accepted 13 Sep 2014; published 13 Oct 2014

Two of the most popular approaches for spectral sensing are monochromators and Fourier transform interferometers. Both require delicate instruments, which limit their use in low-cost applications and tough environments. The key limitation of these methods comes from the fact a long optical path is required to distinguish lights of slightly different wavelengths. Having a long optical path in the free space requires bulky instruments to maintain the alignment. An alternative way to achieve a long optical path in a compact dimension is to have light bounce back and forward many times between interfaces on an integrated optical chip. For example, optical resonators with high quality factors, where light path is enhanced by millions of times compared to the geometrical sizes of the resonators, have been used for spectral sensing [1,2]. However, the operation range is significantly limited by the number of resonators. Here we show a new method of spectral analysis based on the combination of compressive sensing [3] and nanophotonic structures, such as photonic crystal slabs [4]. Nanostructures with their abundant interfaces create much-enhanced optical paths, which is critical to achieve high spectral resolution. More importantly, unlike high-quality resonators whose spectral response consists of discrete narrow lines, the spectral responses of nanostructures are much more random with diverse features due to complex interferences. Such complex responses make it ideal to apply compressive sensing for efficient signal recovery. Using this multiplex method, the operational range is much expanded compared to the high-Q resonator method. These nanostructures can be easily fabricated on a chip and therefore can potentially lead to low-cost, high resolution and compact spectrometers.

Before introducing our method, we first use a general mathematical description to briefly review conventional methods for spectral sensing. We consider an unknown signal light $I(\omega)$ passing through a spectral sensing instrument, whose response function can be described as $R(\omega,\rho)$. Here we use ρ to indicate a particular state of the instrument. A photodetector is used to measure the intensity of transmitted or reflected light $d(\rho)$ as

$$d(\rho) = \int I(\omega) R(\omega, \rho) d\omega \tag{1}$$

Many measurements need to be performed while the instrument is tuned to different states ρ. The measurement $d(\rho)$ can be understood as a transformation of signal $I(\omega)$. The recovery of signal $I(\omega)$ is done through an inverse transformation of the function $d(\rho)$. Different spectral sensing methods use different response functions and accordingly different transformation methods.

A monochromator uses a narrow-band filter based on a highly dispersive optical element, such as grating or prism (Fig. 1(a)). It separates lights of different wavelengths into different directions. A slit is used to selectively let through a narrow band of light around a central frequency ρ. The response function of an ideal monochromator is a delta function (Fig. 1(d))

$$R(\omega, \rho) = \delta(\omega - \rho) \tag{2}$$

Using Eqs. (1) and (2), we have $d(\rho) = I(\rho)$. By measuring the intensity of transmitted light at each frequency ρ, the full spectrum can be obtained directly without an inverse transformation. The resolution of this method scales with the length between the grating and the slit. Since the detector only receives a small portion of signal's energy at each measurement, the noise of detector has a great impact on the performance, making it difficult for infrared regime where the noise of detectors is typically large.

The Fourier transform interferometer has complete different response functions. The signal light is split into two different paths and then is combined (Fig. 1(b)). Because of the interference, $R(\omega,\rho)$ becomes sinusoidal with respect to the frequency (Fig. 1(e)):

$$R(\omega, \rho) = \frac{1 + \cos(\rho\omega)}{2} \tag{3}$$

where ρ is the time delay between two optical paths of the interferometer. Measurements obtained by using different time delay are equivalent to a Fourier transformation of the signal:

#219981 - $15.00 USD Received 29 Jul 2014; revised 12 Sep 2014; accepted 13 Sep 2014; published 13 Oct 2014

$$d(\rho) = \int \frac{1}{2} I(\omega)(1+\cos(\rho\omega))d\omega \qquad (4)$$

The signal can be recovered through an inverse Fourier transformation. For each measurement, significant part of the signal's energy is sent to the detector. Comparing to monochromator, Fourier interferometer has the Fellgett advantage with a better signal-to-noise ratio for infrared light detection [5]. Similar to the monochromator method, the interferometer method also relies on a long and well-aligned optical path, again making it difficult to reduce the footprint without significantly sacrificing the performance.

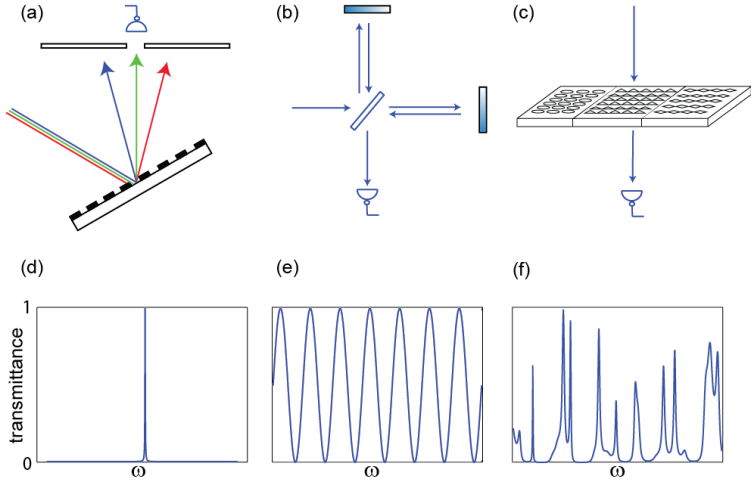

Fig. 1. Monochromator based on grating. b) Fourier transform interferometer. c) compressive sensing using nanophotonic structures. d), e), f) are response functions for a), b), c), respectively.

In this paper, we show a spectral sensing method based on a completely different type of response function, which are obtained by passing the light through a set of different nanophotonic structures (Fig. 1(c)). The transmission and reflection spectra have randomly distributed spectral features (Fig. 1(f)), created by multiple reflections at interfaces of the nanostructure. Response functions at different states ρ are obtained by using different nanophotonic structures and are completely different from each other. They serve as the random bases used in compressive sensing. Before we further describe how to implement nanophotonic structures to generate such random response functions, we first describe the procedure of compressive sensing algorism that will be used to recover the signal I(ω) from the measurement d(ρ).

In compressive sensing, the unknown signal is measured by projecting it to random bases. Typically, the number of measurements is smaller than the dimension of the unknown signal, which requires the signal to be recovered by finding solutions to an underdetermined linear system. It is particularly powerful for recovering sparse signals using less number of measurements than what the Nyquist-Shannon sampling theorem requires. Compressive sensing has been used for advanced imaging [6–12]. Here we use the basis pursuit method described in l_1-magic program for compressive signal recovery [13].

To apply the compressive sensing algorism, we digitize all continuous spectral functions. The spectrum of the signal light is converted to a N-dimension vector $I_n = I(\omega_n)$, $n = 1, \ldots, N$. The random bases, i.e. the response functions of nanostructures, are digitized as $R_{m,n} = R(\omega_n, \rho_m)$ where $m = 1, \ldots, M$, representing M different states of ρ, i.e. M different photonic structures. The measurement is then expressed as $d_m = \sum_n R_{m,n} I_n$. Equation (1) is converted to a set of linear equations with N unknowns and M equations

#219981 - $15.00 USD Received 29 Jul 2014; revised 12 Sep 2014; accepted 13 Sep 2014; published 13 Oct 2014

$$\vec{d} = \vec{\vec{R}}\vec{I} \tag{5}$$

It is always desirable to digitalize the unknown signal with a large N for fine resolution. Therefore, we focus on the case $N > M$ and the linear equations are underdetermined. We can recover the unknown $\vec{I}$ by solving a convex program known as the basis pursuit [14]

$$(P_1) \min \left\| I \right\|_1 \text{ subject to } \vec{d} = \vec{\vec{R}}\vec{I} \tag{6}$$

where $\left\| I \right\|_1 = \sum \left| I_n \right|$ is the l_1 norm of the vector.

Here we want to emphasize that the performance of compressive sensing relies on the randomness of the measuring bases. Therefore, response functions should have diverse spectral features with both broad and narrow line shapes. In addition, different response functions should have minimal correlation. This requirement is difficult to achieve using conventional interferometers consisting of bulk mirrors, lenses or gratings. On the other hand, complex interferences in nanostructures offer extremely rich amount of spectral features. More importantly, the enormous degrees of freedom in choosing the spatial parameters of the nanostructures allow us to create virtually unlimited number of different response functions.

Next, we consider a specific example and use simulations to demonstrate the signal recovery based on compressive sensing. The nanophotonic structure consists of a photonic crystal slab (Fig. 2(a)). It has four layers from the top to the bottom: a 1 μm thick Si layer, a 2.5 μm thick SiO_2 layer, a 0.3 μm thick Si layer and a SiO_2 substrate. A periodic lattice of air holes with a radius r = 0.9 μm are patterned in the top Si layer. The lattice constants in two orthogonal directions are p_1 = 3 μm and p_2 = 3.2 μm. The reflection spectrum (Fig. 2(b)) consists of diverse spectral features. Specifically, the vertical interfaces of air holes cause light to bounce in the lateral direction parallel to the slab. Such lateral propagation forms guided resonances [15], which greatly enhances the optical path with extremely high quality factors. In addition, the slab also has multiple interfaces along the direction normal to the slab. Light bounces between these interfaces, forming Fabry-Perot (FP) resonances. While these FP resonances do not have high quality factors, they play a unique role in enhancing the diversity of spectral features through Fano interference [16]. Fano interference is a result of the interference between guided resonance and direct background transmission. Unlike the symmetrical Lorentz response in regular optical cavities, Fano interference creates highly asymmetrical lineshapes [17,18]. The specific lineshapes depend on the phase and transmittance of the background transmission, which is modulated by the FP resonances. The combination of high-Q guided resonances and low-Q FP resonances through Fano interference leads to diverse spectral features.

We consider a signal light in the spectral range from 1450 nm to 1550 nm. The spectrum is digitalized with 0.1 nm resolution, represented by N = 1001 unknowns to be determined. We use M = 400 different photonic crystal slabs by varying the radius of the holes and the lattice constants. The measurement consists of first passing signal light through each photonic crystal slab and then recording the reflected or transmitted intensity with a photodetector.

These 400 structures have the same layer configuration but with different lattice structures. They are divided into two categories: rectangular and triangular lattices. We use different combinations of hole sizes and lattice constants to obtain different structures and response functions. p_1 varies from 3 μm to 4 μm with a 0.1 μm step. For a given p_1 value, p_2 varies from p_1 to 4 μm with a 0.2 μm step. The diameter of holes ranges from 1.4 μm to p_1 - 1 μm with a 0.2 μm step. We obtain the reflection spectra by solving the Maxwell's equations using rigorous coupled-wave analysis (RCWA). The simulations were performed with *S4* program [19]. A representative spectrum is shown in Fig. 2(b).

To evaluate the performance, we start with an original signal and simulate the measurement processes using Eq. (1). The signal is recovered by feeding d(ρ) into the compressive sensing program implemented in l_1-magic [13]. First, we use a signal consisting of a few continuous waves of different wavelengths. The spectrum consists of a few sharp spikes. We use such signal to evaluate the resolution. The distance between the frequencies of

#219981 - $15.00 USD Received 29 Jul 2014; revised 12 Sep 2014; accepted 13 Sep 2014; published 13 Oct 2014

two continuous waves is 0.1 nm (as shown in Fig. 2(a)). Both the spectral position and the intensity of the signal are recovered well. The resolution is maximized when the spectral features of the response functions are sufficiently complex within certain frequency range. To improve the complexity of the spectra, we need to increase the optical path length, which can be achieved by increasing the number of structural interfaces and the thickness of the structures. For example, by increasing the thickness of top layer photonic crystal slab, or using two layer of different photonic crystal slabs, the resolution can be further improved. In addition, the number of response functions, the sparsity of the signal, and measurement noise also affect the resolution, as expected for any compressive sensing method. The second test signal consists of a broadband Lorentz signal with a 30nm bandwidth and a sharp peak on it. The third test signal combines 17 Lorentzian lines and the fourth combines 5 Gaussian lines. In all cases (Fig. 2(d), 2(e), 2(f)), the original signals are recovered with high fidelity.

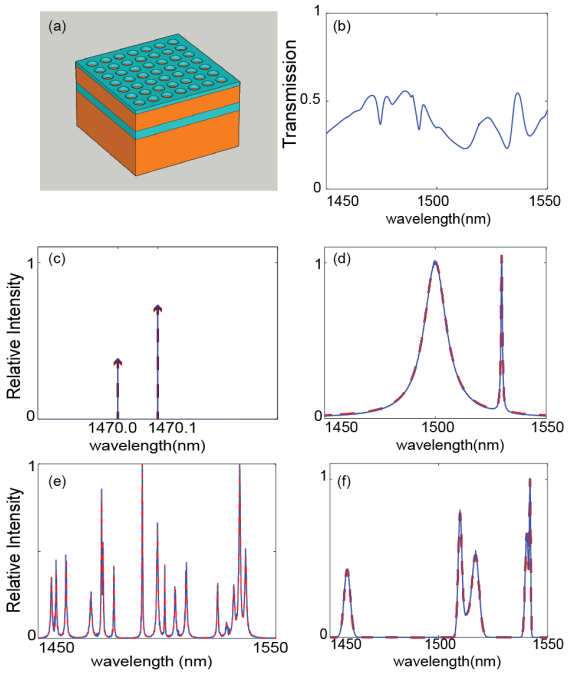

Fig. 2. a) Structure of photonic crystal slab. b) Representative reflection spectrum. c-f) Simulated signal recovery using compressive sensing algorithm and response functions of photonic crystal slabs for c) two discrete peakes d) two Lorentzian lines e) Multiple Lorentzian lines f) five Gaussian lines. The recovered signals (blue solid lines) agree well with the original (red dashed lines).

Even though a large number of different photonic crystal slabs are used, we emphasize that these structures can be readily integrated on a chip. For visible and near-infrared spectral sensing, the required feature sizes can be readily defined by photolithography. The entire chip containing hundreds of different photonic crystal slabs can be as small as a few millimeters. The response functions of these nanostructures will be measured in the calibration process. Unknown signals can then be projected onto the chip and the measurement can be taken in parallel by an array of photodetectors. Alternatively, for weak signals, the measurement can be done sequentially as shown in Fig. 1(c).

In additional to photonic crystal slabs, other nanostructures with complex interferences can also be used to generate random spectral features. For example, multilayer structures with layer thickness ranging from hundreds of nanometers to a few micrometers can generate complex and fine spectral features (Fig. 3).

It is desirable to have minimal correlation among different response functions for the best performance of compressive sensing. Next, we will use the multilayer structure as an example

#219981 - $15.00 USD Received 29 Jul 2014; revised 12 Sep 2014; accepted 13 Sep 2014; published 13 Oct 2014

to evaluate the impact of correlation. We compare two types of multilayer structures, both consisting of 5 layers of silicon slabs with air spacing. For the first type (Fig. 3(a)), all 5 layers have the same thicknesses of 15 μm. Different response functions are obtained by randomly varying the thicknesses of air spacing between layers in the range from 3 – 4 μm. Figure 3(b)-(e) show three representative spectra. By examining these spectra, we recognize that despite different detailed features, they all share a common pattern with a spectral periodicity determined by the FP resonance of the 15 μm thick Si slab. We can evaluate the correlation among different spectral response defined as

$$C_{i,j} = \frac{E[(\mathrm{R}(\omega,\rho_i) - E(\mathrm{R}(\omega,\rho_i)))(\mathrm{R}(\omega,\rho_j) - E(\mathrm{R}(\omega,\rho_j)))]}{\sqrt{E[(\mathrm{R}(\omega,\rho_i) - E(\mathrm{R}(\omega,\rho_i)))^2]\,\mathrm{E}[(\mathrm{R}(\omega,\rho_j) - E(\mathrm{R}(\omega,\rho_j)))^2]}} \tag{7}$$

where $E(.)$ represents the average. We obtain the response functions by simulating 400 different structures using *S4* [19]. The average correlation is 0.74, indicating significant similarity among different response functions. Using this set of response functions, we apply the compressive sensing algorithm for a signal consisting of 5 Lorentzian peaks (Fig. 3(e), red line). The peak positions and heights are barely recovered (Fig. 3(e), blue line).

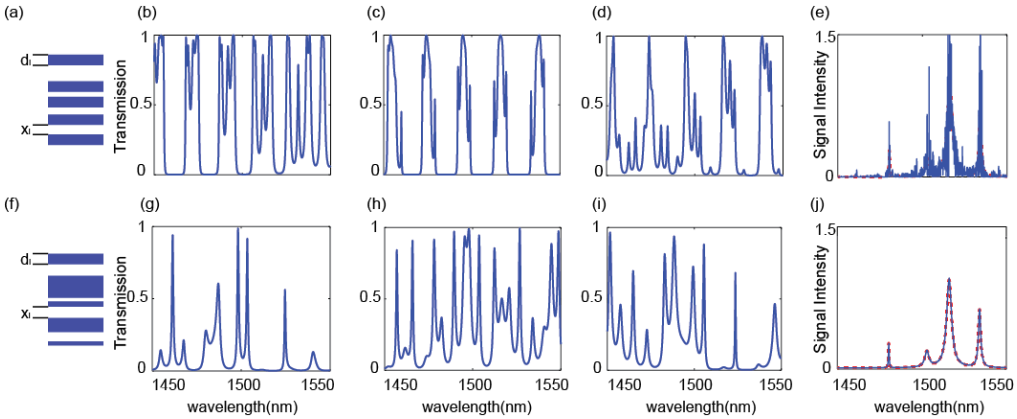

Fig. 3. The performance of the signal recovery depends on the implementation of the response functions. a) The multi-layer structure that generates the response functions have 5 Si layers (blue slabs) with the same thickness of 15μm. The distances are varied to obtain 400 different structures. b-d) three representative response functions. e) the recovered signal barely reproduces the original signal with a high noise level. f) Both the thicknesses and the distances between layers are varied. g-i) three representative response functions for f). j) the recovered signal agrees well with the original signal.

For the second type of structures (Fig. 3(f)), we obtain 400 different response functions by changing both the thickness of and the spacing between Si layers. The spacing is randomly chosen between 3 to 4 μm and the thickness is randomly chosen between 10 nm to 15 μm. Figure 3(g)-(i) show representative spectra. The average correlation for 400 different response functions is 0.01, much smaller than that of the first type of structures. Figure 3(j) shows that the same signal now is very well recovered by this set of response functions. The comparison between these two types of structures shows the importance of correlation in designing photonic structures.

Finally, we use the second type of multi-layer structure to evaluate the tolerance of measurement noise. Noise is inevitable in every step of experimental measurement. In the simulation, a random noise is added to the response functions. This noise could come from the experimental measurement of the response functions during the initial calibration of the instrument. Specifically, we have

$$R'(\omega,\rho) = R(\omega,\rho) + \delta R(\omega,\rho) \tag{8}$$

#219981 - $15.00 USD Received 29 Jul 2014; revised 12 Sep 2014; accepted 13 Sep 2014; published 13 Oct 2014

where $R(\omega,\rho)$ is the true response function and $R'(\omega,\rho)$ is the measured response function. $\delta R(\omega,\rho)$ is the random noise. The measurement of the signal passing through the photonic structure also induces a noise given by $\delta \mathrm{d}(\rho)$

$$d'(\rho) = \int I(\omega) R(\omega,\rho)\,\mathrm{d}\omega + \delta \mathrm{d}(\rho) \tag{9}$$

$I'(\omega)$ is recovered by compressive sensing algorithm using measured data $R'(\omega,\rho)$ and $d'(\rho)$. Figure 4(a) shows the case without noise. Figure 4(b) shows the noisy case with a signal-to-noise ratio of 40dB, e.g. the ratios between δR and R and between δd and d. In both cases, $I'(\omega)$ (blue solid line) agrees well with $I(\omega)$ (red dashed line). The noise tolerance highly depends the algorithm used for the signal recovery. The linear programming described here in Eq. (6) is not designed for recovering noisy signal. The noise tolerance can be further improved by using a quadratic instead of the equality constraint [13]. In addition to the measurement noise, drift of the response function induced by temperature change is also common in spectral sensing. A known reference light beam or temperature sensors can be implemented to monitor such drift and compensate the measured spectra accordingly.

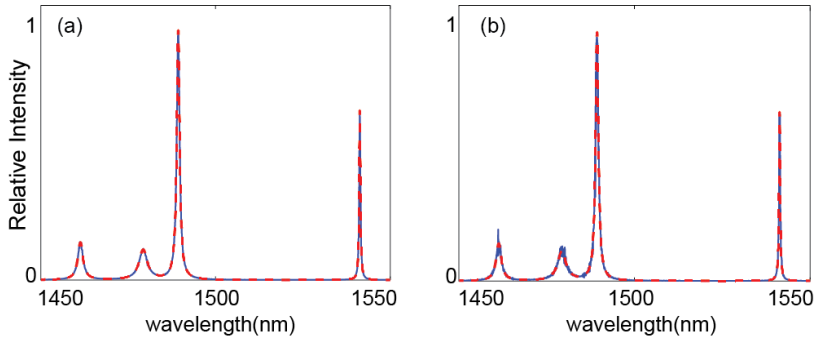

Fig. 4. Result of signal recovery using compressive sensing without noise (a) and with noise (b). Red dashed lines are the original signals, and blue solid lines are the recovered signals.

Acknowledgments

The work was supported by the Wisconsin Alumni Research Foundation and partially by the Office of Naval Research under grant number N00014-14-1-0300. Z. Wang acknowledges the help from M. Zhou for simulation setup.